Supplementary Information S1

LC-MS/MS and high-spatial single-cell MALDI-MSI reveal selective downregulation of PC(16:0_16:0) and PC(18:0_18:1) due to mPGES-1 knockdown in hormone-resistant prostate cancer cell line

Mst. Sayela Afroz[1], Shuhei Aramaki[2,3]*, Md. Muedur Rahman[1,4], Maxime Dubail[1], Md. Al Mamun[4,5], Takumi Sakamoto[1,4], Zhang Chi[1], Kyoka Fujii[6], Mariko Kurosawa[6], Keita Tamura[7], Tomohito Sato[1], Yutaka Takahashi[1,4], Tomoaki Kahyo[1,8], Katsumasa Nakamura[3], Teruo Inamoto[7], Olof Rådmark[9], Mitsutoshi Setou[1,10], Hiromi Hanaka[6]*

1. Department of Cellular and Molecular Anatomy, Hamamatsu University School of Medicine, 1-20-1 Handayama, Chuo-ku, Hamamatsu, Shizuoka 431-3125, Japan
2. Photonic Quantum Therapeutics Laboratory, Institute of Photonics Medicine, Hamamatsu University School of Medicine, 1-20-1 Handayama, Chuo-ku, Hamamatsu, Shizuoka 431-3125, Japan
3. Department of Radiation Oncology, Hamamatsu University School of Medicine, 1-20-1 Handayama, Chuo-ku, Hamamatsu, Shizuoka 431-3125, Japan
4. Preppers Co., Ltd., 1-20-1 Handayama, Chuo-ku, Hamamatsu, Shizuoka 431-3125, Japan
5. Cancer Center, Medical College of Wisconsin, 8701 Watertown Plank Road, Milwaukee, Wisconsin, 53226, USA.
6. Graduate School of Life Science, Showa Women's University, 1-7-57 Taishido, Setagaya-Ku, Tokyo, Japan.
7. Department of Urology, Hamamatsu University School of Medicine, 1-20-1 Handayama, Chuo-ku, Hamamatsu, Shizuoka 431-3125, Japan
8. Quantum Imaging Laboratory, Division of Research and Development in Photonics Technology / International Mass Imaging and Spatial Omics Center, Institute of Photonics Medicine, 1-20-1 Handayama, Chuo-ku, Hamamatsu, Shizuoka 431-3125, Japan
9. Department of Medical Biochemistry and Biophysics, Division of Physiological Chemistry II, Karolinska Institute, 171 77, Stockholm, Sweden
10. International Mass Imaging and Spatial Omics Center, Institute of Photonics Medicine, 1-20-1 Handayama, Chuo-ku, Hamamatsu, Shizuoka 431-3125, Japan

Author of Correspondence*

Shuhei Aramaki
Photonic Quantum Therapeutics Laboratory, Institute of Photonics Medicine, Hamamatsu University School of Medicine, 1-20-1 Handayama, Chuo-ku, Hamamatsu, Shizuoka 431-3125, Japan
Email: aramaki@hama-med.ac.jp; Phone: +81-053-435-2086; Fax: +81-053-435-2468

Hiromi Hanaka
Graduate School of Life Science, Showa Women's University, 1-7-57 Taishido, Setagaya-Ku, Tokyo, Japan.
Email: h-hanaka@swu.ac.jp; Tel: +81-03-3411-7450, Fax: +81-03-3411-7428

List of content:

Fig. S3 Ion images and corresponding mass spectra of the spatial distribution of lipid molecules in the MPGES-1 KD, WT, and NC DU145 cells at the single-cell level measured by AP-MALDI mass microscope in positive ion mode. **a** Ion image of PC (16:1_18:1) at *m/z* 758.55 $[M+H]^+$, **b** Ion image of PC (16:0_20:4) at *m/z* 782.56 $[M+H]^+$, **c** Ion image of PC (40:8) at *m/z* 868.52 $[M+K]^+$, **d** Ion image of PC (38:4) at *m/z* 810.60 $[M+H]^+$; **e** DG (O-36:4) at *m/z* 603.52 $[M+H]^+$; **f** DG(35:3) at *m/z* 605.54; **g** DG (37:6) at *m/z* 627.51; **h** PC (16:1_17:1) at *m/z* 744.56; **i** PC (42:10) at *m/z* 854.56; and **j** PC (44:10) at *m/z* 882.58

Table S5. Detection of different lipid classes measured in LC-MS and MALDI-MSI analysis.

Table S6. This table shows the changes in arachidonic-acid-containing lipid molecules in KD compared to controls observed in LC-MS/MS analysis.

Fig. S7 Statistical analysis of the arachidonic acid-containing lipid molecules among KD, WT, and NC cells. **a** Ion image and histogram of the intensity distribution of PC (16:0/20:4) at the single-cell level analysis showed a significant difference in KD compared to WT and NC, but also showed a significant difference between WT vs NC. **b** Ion image and histogram of the intensity distribution of PC (18:0/20:4) at the single-cell level analysis showed no significance among the groups. Kruskal-Wallis significance test. P. adj <=0.0001~****, P. adj <=0.001~***, P. adj <=0.01~**, P. adj <=0.05~*.

Fig. S8 H&E image showing the laser pixel within a cell

Fig. S9 PGE2 exerts its role in phosphatidylcholine synthesis and its consequences in prostate cancer. PGE2 transmits its signal through G-protein-coupled cell surface receptors (EP1 to EP4). After PGE2 binding to the EP receptors, various intracellular oncogenic pathways are stimulated. PGE2 binding with EP4 stimulated the PI3K/Akt pathway through cyclooxygenase pathways independently, which enhances the activity of choline kinase (CK) and Choline phosphate cytidylyltransferase-α (CCTα), resulting in the upregulation of PC biosynthesis. In hormone-resistant prostate cancer cell PC(16:0_16:1), PC(18:10_18:1) are markedly increased, but due to knockdown of the mPGES1 gene in hormone-resistant prostate cancer cells, these two lipids are significantly downregulated in the KD group compared to the WT and NC groups.

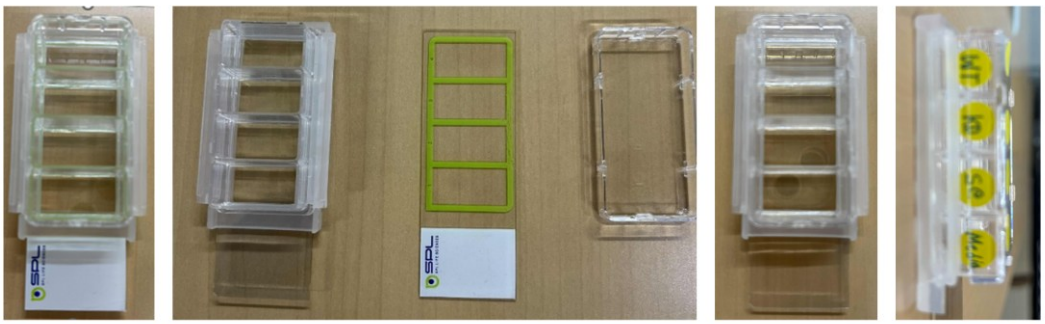

(a) Chambered Normal Slide

(b) Reassemble the Chambered Slide using an ITO-coated slide

(c) Chambered ITO-coated Slide

(d) Marked the chamber for cell culture

Fig. S1: The chambered slide was reassembled to incorporate the ITO-coated slide for cell culture and the MALDI-MSI experiment.

Table S1: LipidSearch (version 5.1) software parameters

Search parameters	**Settings**
Target database	HCD
Search type	Product
Experiment type	LC-MS/MS
Precursor tolerance	5.0 ppm
Product tolerance	8.0 ppm
Intensity threshold (relative)	0.01% (parent), 0.1% (product)
m-score threshold	2.0
Recalc isotype	on
RT interval (min)	0.0
Quantitation	**Settings**
Execute quantitation	on
m/z tolerance	±5.0 ppm
RT range	±0.5 min
Filters	Settings
Toprank filter	on
Main node filter	Main isomer peak
m-score threshold	2.0
c-score threshold	2.0
FA polarity	on

ID quality filter	A, B, and C
Class	**Settings**
Lipid class	All
Adducts	**Settings**
Positive	+H, +NH4, +Na, +K, +H-H2O, +H-2H2O
Negative	-H, +HCOO, +CH3COO
Alignment parameters	**Settings**
Search type	Product
Experiment type	LC-MS/MS
Alignment method	Max
RT tolerance	0.25 min
Calculate the unassigned peak area	on
Filter type	New filter
Toprank filter	on
Main node filter	Main isomer peak
m-score threshold	2.0
ID quality filter	A, B, and C

Table S2. This table showed ceramide and other lipids that were significantly altered in KD compared to WT and NC, but WT did not show significant changes compared to NC, as observed in LC-MS analysis.

Lipid Molecules	FC KD/WT	FC KDvsNC	FC WTvsNC	P-value KDvsWT	p-value KDvsNC	P-value WTvsNC
Cer(d18:0_14:0)	4.60	5.38	1.17	<0.001	0.001	0.350
Cer(d18:0_16:0)	2.49	4.25	1.71	<0.001	<0.001	0.054
Cer(d18:1_24:0)	2.32	3.50	1.51	<0.001	0.001	0.124
Cer(t18:0_23:2)	0.46	0.41	0.90	0.021	0.056	0.390
LBPA(18:0_18:1)	2.73	3.43	1.25	<0.001	<0.001	0.144
SM(d38:2)	0.24	0.29	1.24	0.002	0.007	0.162

Statistical evaluation was conducted using Welch's t-test, followed by the Benjamini–Hochberg method. T-test. significant, $P < 0.05$, $|log2FC|>0.5$.

Table S3. Neutral lipids were significantly downregulated in KD compared to WT and NC, but WT did not show significant changes compared to NC, as observed in LC-MS analysis.

Lipid Molecules	FC KD/WT	FC KDvsNC	FC WTvsNC	P-value KDvsWT	P-value KDvsNC	P-value WTvsNC
DG(18:0_20:2)	0.43	0.43	0.99	0.010	0.015	0.478
DG(18:1_19:1)	0.48	0.44	0.92	0.012	0.040	0.381
DG(18:1_20:1)	0.45	0.43	0.95	0.007	0.010	0.415
DG(18:1_22:2)	0.46	0.38	0.82	0.004	0.039	0.276
DG(18:1_22:3)	0.48	0.35	0.73	0.001	0.039	0.195

DG(18:1_24:3)	0.44	0.35	0.81	0.008	0.019	0.240
DG(20:2_18:1)	0.42	0.48	1.13	0.033	0.018	0.348
DG(22:5_24:4)	0.24	0.17	0.72	0.011	0.104	0.327
DG(O-15:0_23:3)	0.48	0.29	0.62	0.018	0.055	0.176
TG(16:0_16:0_26:1)	0.44	0.43	0.97	0.037	0.044	0.453
TG(16:0_18:0_26:1)	0.41	0.42	1.04	0.041	0.051	0.433
TG(16:0_18:1_25:1)	0.49	0.38	0.77	0.023	0.029	0.196
TG(16:0_18:1_26:1)	0.43	0.35	0.81	0.011	0.019	0.213
TG(16:0_18:1_27:1)	0.43	0.33	0.77	0.012	0.030	0.207
TG(16:0_18:1_32:1)	0.29	0.36	1.24	0.007	0.020	0.127
TG(16:0_20:1_26:1)	0.39	0.36	0.93	0.017	0.022	0.367
TG(16:0_25:0_18:1)	0.46	0.44	0.95	0.026	0.051	0.417
TG(18:0_26:0_18:1)	0.35	0.37	1.05	0.029	0.029	0.403
TG(18:1_18:1_23:1)	0.48	0.26	0.54	0.022	0.030	0.097
TG(18:1_18:1_24:2)	0.48	0.24	0.51	0.034	0.017	0.063
TG(18:1_18:1_25:1)	0.45	0.29	0.64	0.018	0.027	0.127
TG(18:1_18:1_26:1)	0.39	0.31	0.79	0.004	0.009	0.164
TG(18:1_18:1_26:2)	0.44	0.25	0.58	0.023	0.024	0.102
TG(18:1_18:1_27:1)	0.47	0.34	0.73	0.014	0.027	0.159
TG(18:1_18:1_27:1)	0.48	0.33	0.70	0.014	0.014	0.110
TG(18:1_18:1_28:1)	0.42	0.34	0.82	0.007	0.012	0.190
TG(18:1_18:1_30:1)	0.40	0.38	0.95	0.009	0.013	0.386
TG(18:1_20:1_20:1)	0.48	0.26	0.55	0.042	0.020	0.083
TG(22:0_22:2_22:2)	0.40	0.31	0.78	0.010	0.010	0.146
TG(25:0_18:1_18:1)	0.46	0.36	0.78	0.014	0.018	0.182
TG(34:1_30:1)	0.36	0.37	1.03	0.014	0.020	0.429
TG(46:5_16:0)	0.40	0.37	0.92	0.005	0.019	0.356
TG(56:2_6:0)	0.49	0.40	0.82	0.013	0.026	0.240
TG(O-9:0_12:0_3:0)	0.01	0.01	1.24	0.008	0.185	0.412

Statistical evaluation was conducted using Welch's t-test, followed by the Benjamini–Hochberg method. T-test. significant, $P < 0.05$, $|log2FC|>0.5$.

Table S4. This table showed the significantly altered phosphatidyl-containing lipid molecules in KD compared to WT and NC. Still, WT did not show significant changes compared to NC, as identified in LC-MS analysis.

Lipid Molecules	**FC KDvsWT**	**FC KDvsNC**	**FC WTvsNC**	**P-value KDvsWT**	**p-value KDvsNC**	**P-value WTvsNC**
LPC(20:2)	0.41	0.39	0.94	0.034	0.067	0.444
LPC(20:2)	0.41	0.39	0.94	0.034	0.067	0.444
PC(13:0_18:0)	0.49	0.44	0.91	0.002	0.031	0.344
PC(16:0_16:0)	**0.48**	**0.45**	**0.94**	**<0.001**	**0.037**	**0.299**
PC(18:0_18:1)	**0.49**	**0.49**	**0.99**	**0.002**	**0.001**	**0.340**
PC(18:1_18:4)	0.41	0.49	1.19	0.013	0.126	0.319
PC(34:4)	0.40	0.46	1.14	0.038	0.084	0.320
PC(35:0)	0.46	0.36	0.78	0.009	0.046	0.254
PC(41:1)	0.48	0.46	0.97	0.013	0.065	0.460

PC(48:6)	0.37	0.43	1.16	0.031	0.017	0.330
PC(O-15:1_26:1)	0.42	0.32	0.76	0.010	0.040	0.230
PC(O-16:0_24:5)	0.35	0.30	0.86	<0.001	0.153	0.414
PC(O-18:3_24:5)	0.29	0.43	1.49	0.033	0.059	0.147
PC(O-33:0)	0.49	0.49	0.99	0.014	0.067	0.488
PC(O-33:1)	0.45	0.42	0.91	0.006	0.023	0.360
PC(O-35:0)	0.30	0.19	0.63	0.009	0.038	0.172
PC(O-37:0)	0.45	0.43	0.97	0.022	0.071	0.465
PC(O-39:6)	0.36	0.42	1.16	0.023	0.022	0.240
PC(O-42:0)	0.36	0.46	1.27	0.015	0.029	0.186
PE(44:1)	0.48	0.39	0.82	0.023	0.015	0.178
PE(O-17:1_18:1)	2.17	2.17	1.00	0.004	<0.001	0.498
PE(O-17:2_18:1)	4.03	5.20	1.29	0.006	0.004	0.311
PE(O-18:1_26:1)	0.42	0.30	0.71	0.008	0.061	0.232
PE(O-37:1)	0.49	0.44	0.89	0.005	0.009	0.287
PE(P-18:0_26:1)	0.39	0.29	0.75	0.010	0.060	0.266
PEt(O-15:1_24:6)	0.41	0.37	0.91	0.009	0.086	0.411
PEt(P-11:0_21:1)	2.10	2.96	1.41	0.037	0.004	0.240
PG(18:0_18:1)	2.13	2.47	1.16	<0.001	0.001	0.263
PG(28:0)	4.19	2.13	0.51	0.005	0.063	0.222
PG(O-17:1_23:7)	0.47	0.36	0.78	0.027	0.029	0.239
PG(P-11:0_18:2)	3.29	2.76	0.84	0.043	0.055	0.266
PG(P-11:0_18:2)	3.37	2.66	0.79	0.001	<0.001	0.225
PI(18:0_22:5)	2.04	2.05	1.00	0.024	0.027	0.497
PI(18:0_22:6)	2.22	2.75	1.24	0.027	0.018	0.056
PI(18:2_18:0)	2.70	3.38	1.25	0.011	0.005	0.294

Statistical evaluation was conducted using Welch's t-test, followed by the Benjamini–Hochberg method. T-test. significant, $P < 0.05$, $|log2FC|>0.5$.

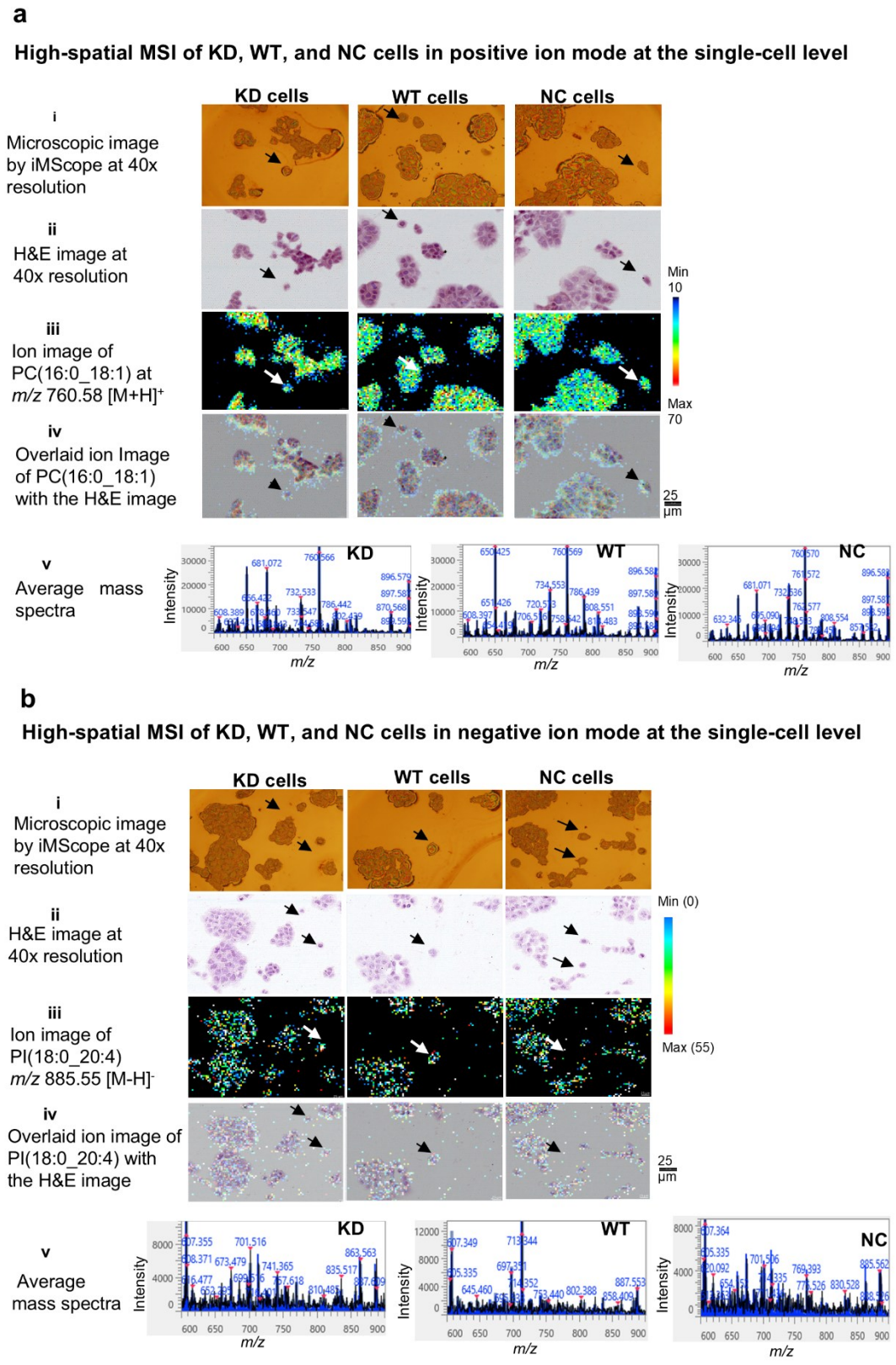

Fig. S2 Single-cell MALDI-MSI of DU145 mPGES-1 KD, WT, and NC cells to visualize the spatial distribution of lipid molecules at the single-cell level, both in positive and negative ion mode by AP-

MALDI mass microscope, where both clusters of cells and single cells (white and black arrows) are shown. **a.i** and **b.i** Microscopic image of KD, WT, and NC cells by embedded microscope of iMScope instrument before matrix deposition at 40x resolution; **a.ii** and **b.ii** H&E image of the cells after MALDI-MSI measurement; **a.iii** and **b.iii** Ion image of PC(16:0/18:1) at *m/z* 760.58 $[M+H]^+$ and PI(18:0/20:4) at *m/z* 885.55 $[M-H]^-$; **a.iv** Overlaid ion image of PC(16:0/18:1) with the H&E image and **b.iv** overlaid ion image of PI(18:0/20:4) with the ion image. **a.v** and **b.v** Average mass spectra.

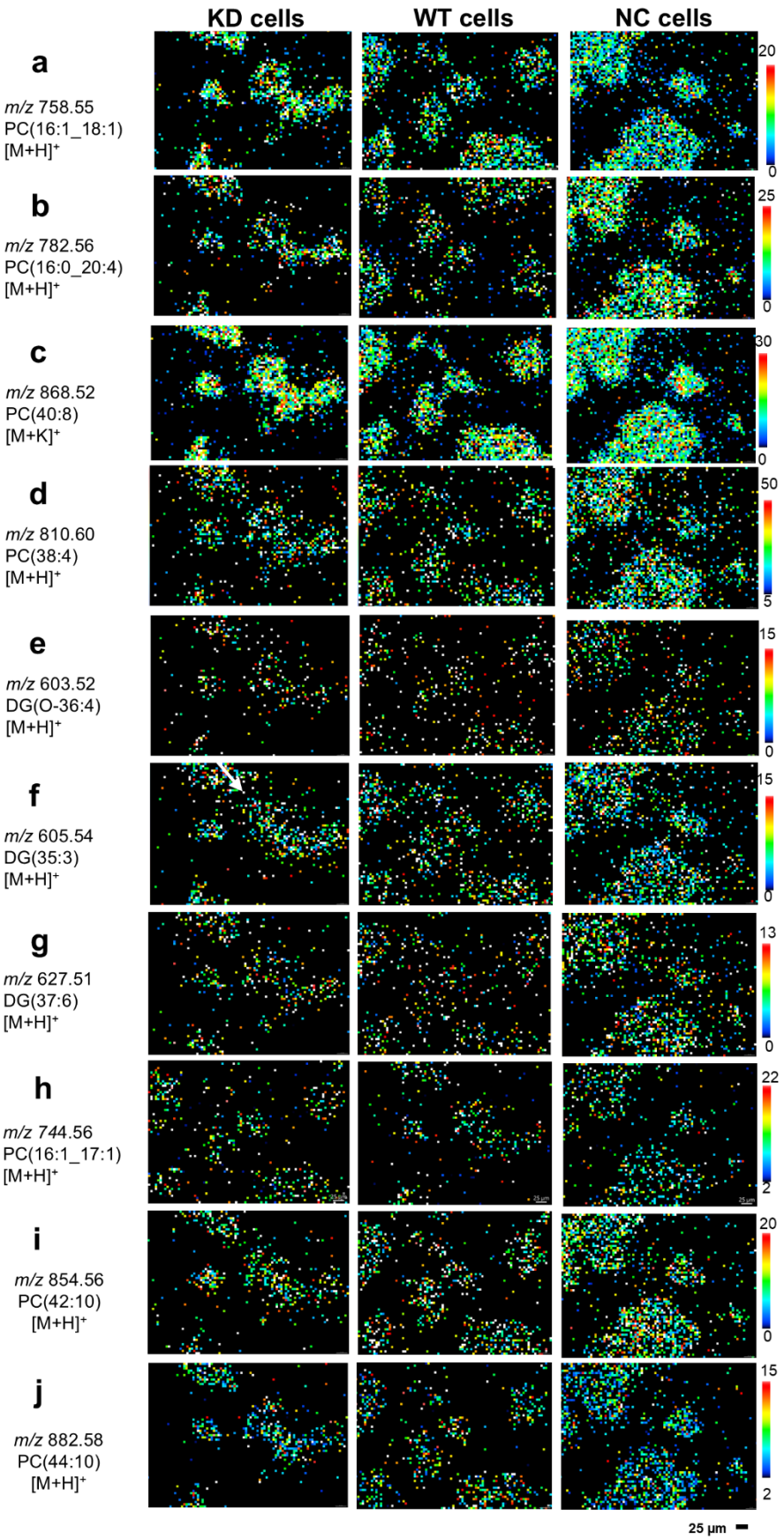
KD cells
WT cells
NC cells
a
m/z 758.55
PC(16:1_18:1)
[M+H]+
20
0
b
m/z 782.56
PC(16:0_20:4)
[M+H]+
25
0
c
m/z 868.52
PC(40:8)
[M+K]+
30
0
d
m/z 810.60
PC(38:4)
[M+H]+
50
5
e
m/z 603.52
DG(O-36:4)
[M+H]+
15
0
f
m/z 605.54
DG(35:3)
[M+H]+
15
0
g
m/z 627.51
DG(37:6)
[M+H]+
13
0
h
m/z 744.56
PC(16:1_17:1)
[M+H]+
22
2
i
m/z 854.56
PC(42:10)
[M+H]+
20
0
j
m/z 882.58
PC(44:10)
[M+H]+
15
2
25 µm

Fig. S3 Ion images and corresponding mass spectra of the spatial distribution of lipid molecules in the MPGES-1 KD, WT, and NC DU145 cells at the single-cell level measured by AP-MALDI mass microscope in positive ion mode. **a** Ion image of PC (16:1_18:1) at *m/z* 758.55 $[M+H]^+$, **b** Ion image of PC (16:0_20:4) at *m/z* 782.56 $[M+H]^+$, **c** Ion image of PC (40:8) at *m/z* 868.52 $[M+K]^+$, **d** Ion image of PC (38:4) at *m/z* 810.60 $[M+H]^+$; **e** DG (O-36:4) at *m/z* 603.52 $[M+H]^+$; **f** DG(35:3) at *m/z* 605.54; **g** DG (37:6) at *m/z* 627.51; **h** PC (16:1_17:1) at *m/z* 744.56; **i** PC (42:10) at *m/z* 854.56; and **j** PC (44:10) at *m/z* 882.58

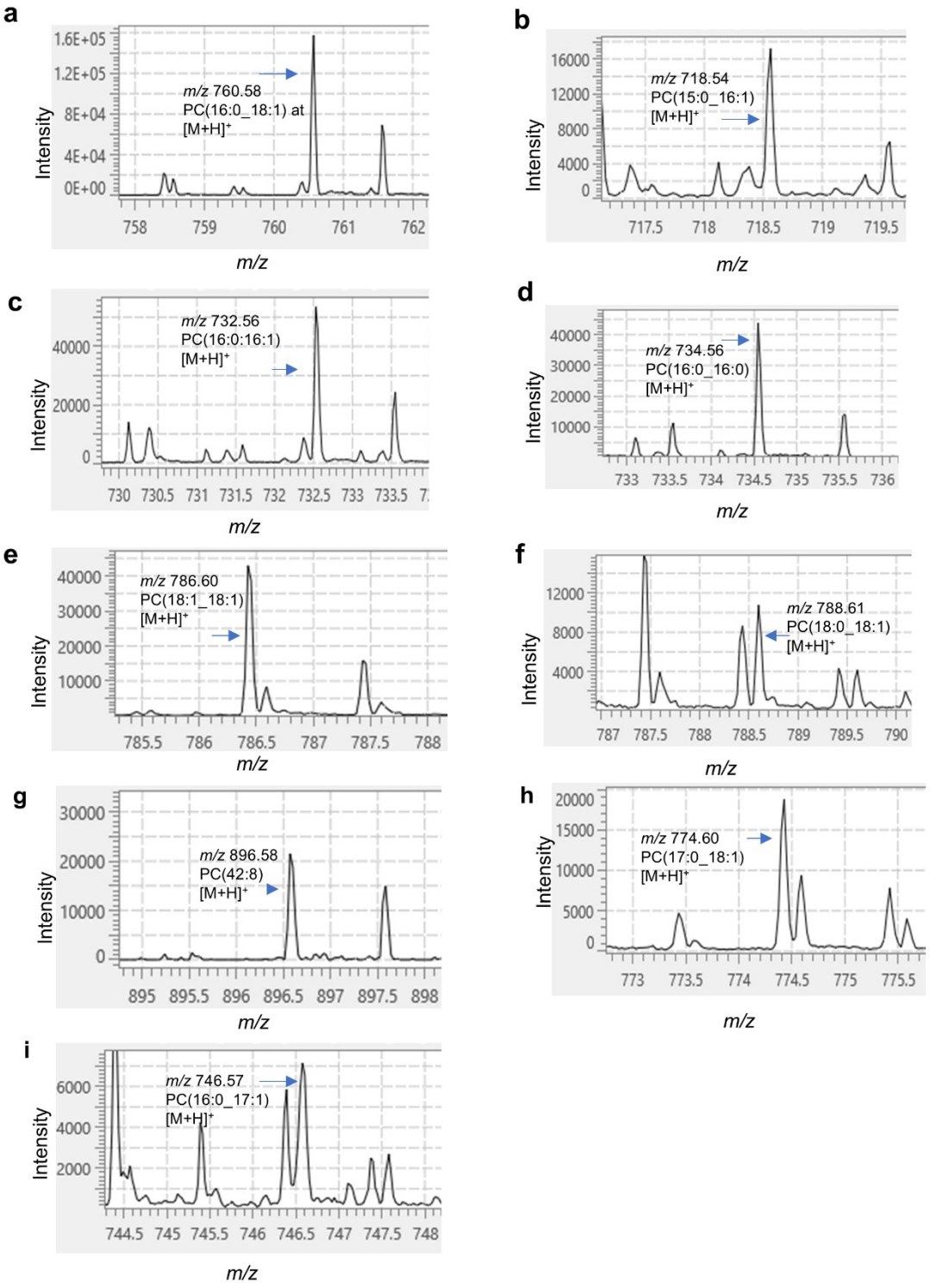

Fig. S4 Corresponding mass spectra of the PC(16:0_18:1), PC(15:0_16:1), PC(16:0_16:1), PC(16:0_16:0), PC(18:1_18:1), PC(18:0_18:1), PC(42:8), PC(17:0_18:1), and PC(16:0_17:1) at *m/z* 760.58 $[M+H]^+$, 718.54 $[M+H]^+$, 732.56 $[M+H]^+$, 734.56 $[M+H]^+$, 786.60 $[M+H]^+$, 788.61 $[M+H]^+$, 896.58 $[M+H]^+$, 774.60 $[M+H]^+$, and 746.57 $[M+H]^+$ respectively observed in the spatial MSI analysis.

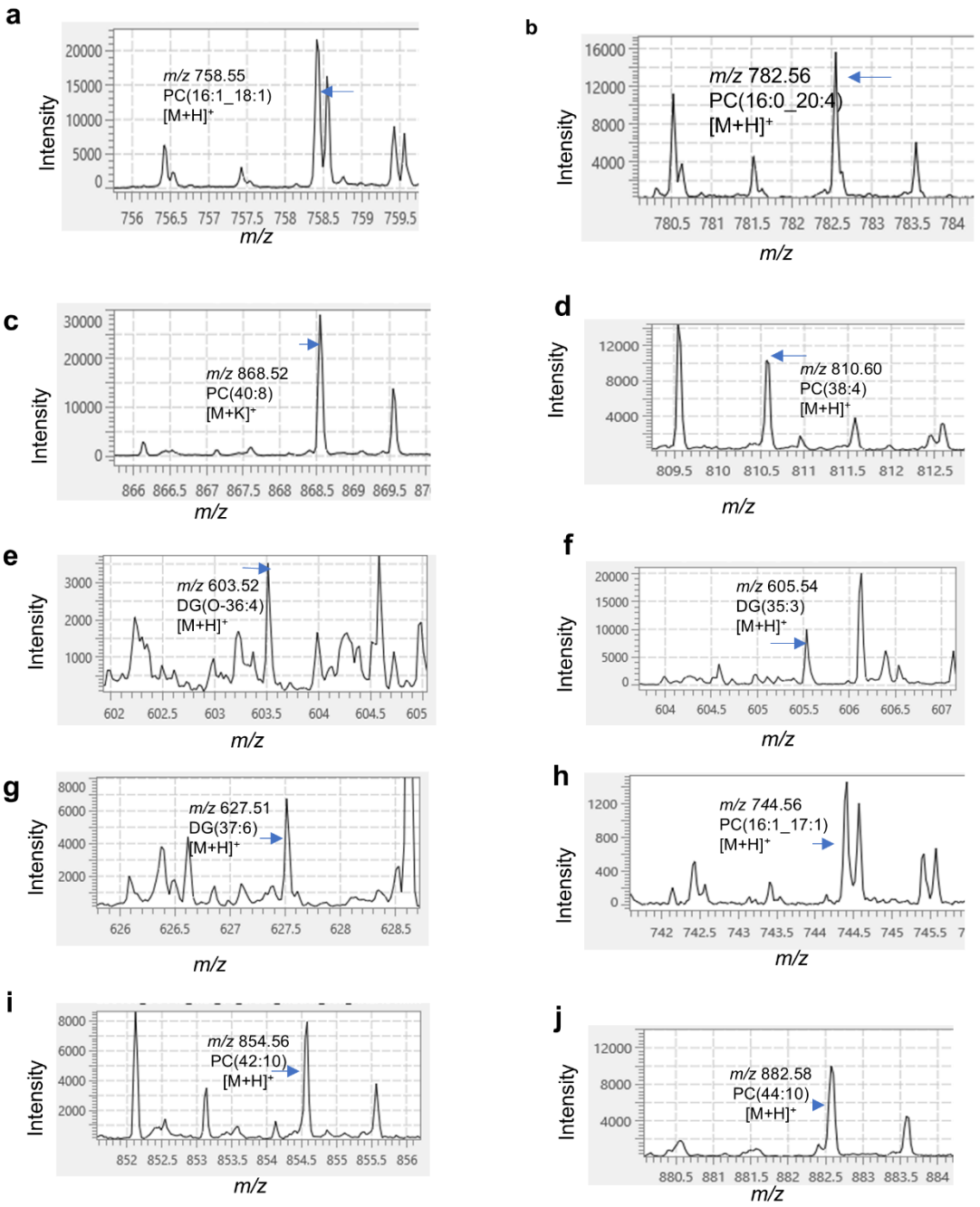

Fig. S5 Corresponding mass spectra of the PC (16:1_18:1), PC (16:0_20:4), PC (40:8), PC (38:4), DG (O-36:4), DG(35:3), DG (37:6), PC (16:1_17:1), PC (42:10), PC (44:10), respectively obtained in spatial MSI analysis.

i. Representative ion images measured by AP-MALDI at negative ion mode

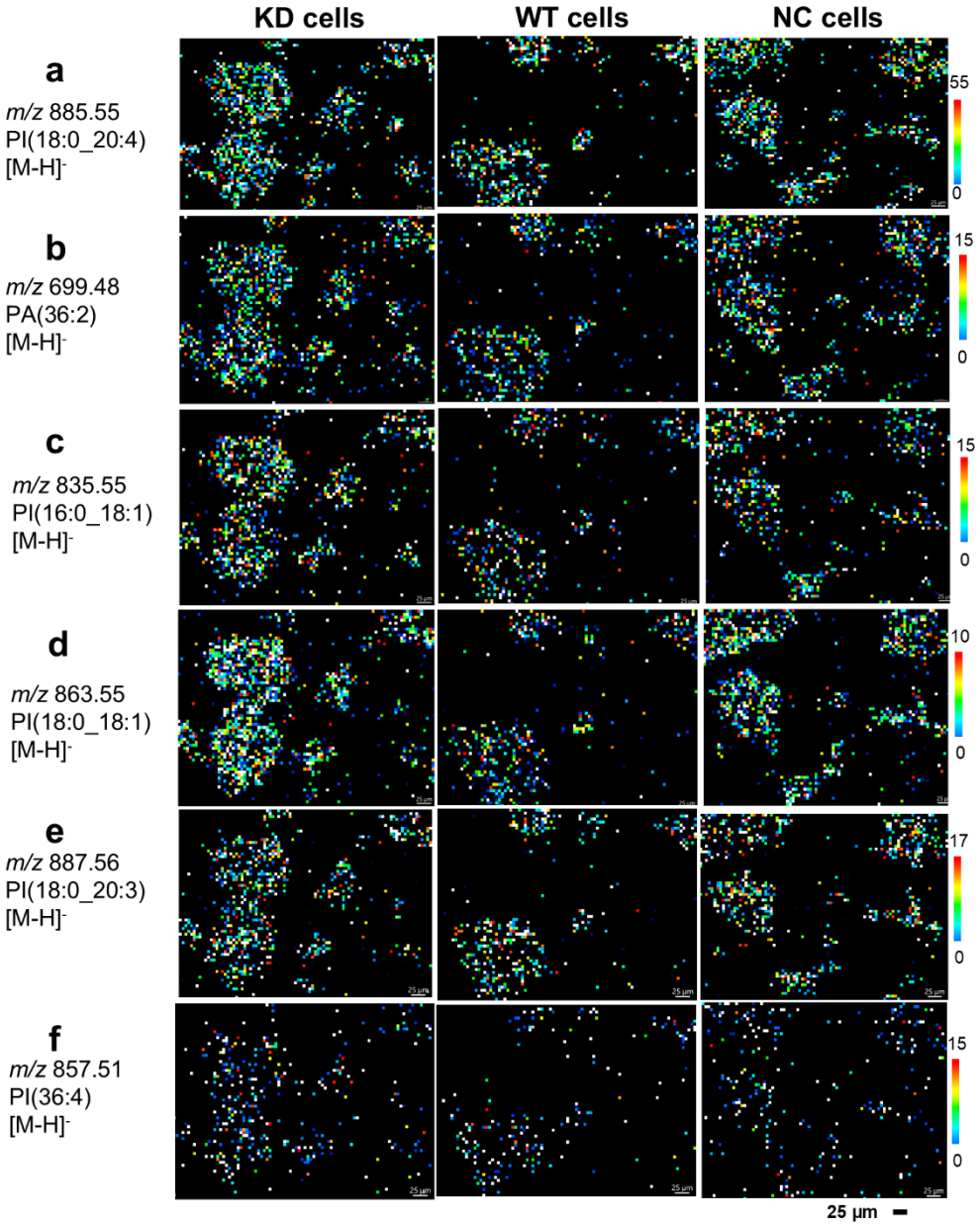

ii. Corresponding mass spectra of the representative ion images

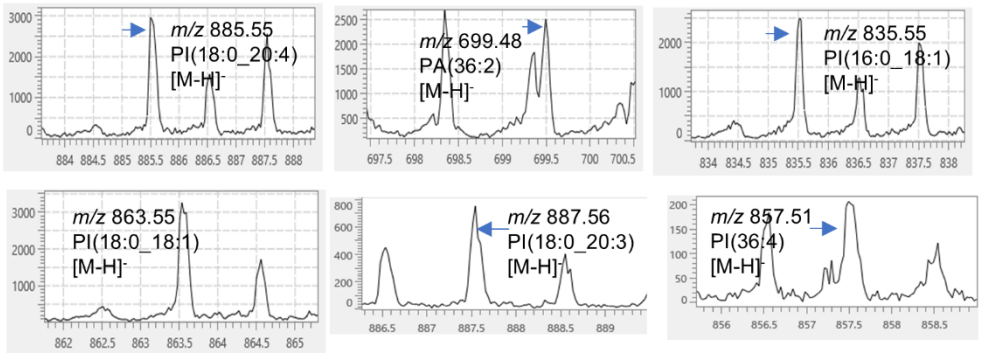

Fig. S6 Ion images and corresponding mass spectra of the spatial distribution of lipid molecules of DU145 mPGES-1 KD, WT, and NC cells measured by AP-MALDI mass microscope in negative ion mode at the single-cell level; **a** PI(18:0_20:4) at *m/z* 885.55 $[M-H]^-$, **b** PA (36:2) at *m/z* 699.48 $[M-H]^-$ **c** PI (16:0_18:1) at *m/z* 835.55 [M-H]; **d** PI(18:0_18:1) at *m/z* 863.55 [M-H]; **e** PI(18:0_20:3) at *m/z* 887.56 $[M-H]^-$ and **f** PI(36:4) at *m/z* 857.51 $[M-H]^-$.

Table S5. Detection of different lipid classes measured in LC-MS and MALDI-MSI analysis.

Lipids	**LC-MS analysis**	**MALDI-MSI analysis**	**Common in both modalities**
Lipid classes and species obtained	PC, PE, PI, PS, PG, PA, DG, TG, Cer, SM, and arachidonic-acid-containing lipid species	PC, PI, PA, and arachidonic-acid-containing lipid species	PC, PI, PA, and arachidonic-acid-containing lipid species
Up and down-regulated lipid classes (Mainly)	↓PC, ↓TG, and ↑Cer	↓PC	↓PC
Abbreviations: Glycerophosphocholines (PC), Glycerophosphoethanolamines (PE), Glycerophosphoinositols (PI), Glycerophosphoserines (PS), Glycerophosphoglycerols (PG), Glycerophosphates (PA), Diradylglycerolipids (DG), Triradylglycerolipids (TG), Ceramides (Cer), Sphingomyelins (SM) Lipid class name according to the LIPIDMAPS database.			

Table S6. This table shows the changes in arachidonic-acid-containing lipid molecules in KD compared to controls observed in LC-MS analysis.

LipidMolecules	**FC KDvsWT**	**FC KDvsNC**	**FC WTvsNC**	**P-value KDvsWT**	**p-value KDvsNC**	**P-value WTvsNC**
PC(18:0/20:4)	0.66	0.61	0.92	0.078	0.072	0.395
PC(18:1/20:4)	1.00	0.90	0.90	0.495	0.307	0.332
PC(O-13:1/20:4)	1.13	1.37	1.22	0.144	0.069	0.150
PC(O-18:1/20:4)	0.86	0.84	0.97	0.127	0.136	0.430
PE(14:0/20:4)	1.19	1.09	0.91	0.119	0.379	0.385
PE(16:0/20:4)	1.41	1.31	0.93	0.006	0.143	0.392
PE(16:1/20:4)	0.93	0.98	1.05	0.287	0.465	0.415
PE(17:0/20:4)	1.03	0.98	0.95	0.364	0.427	0.350
PE(18:0/20:4)	1.24	1.30	1.05	0.017	0.054	0.368
PE(18:1/20:4)	0.86	0.70	0.82	0.149	0.129	0.251
PE(24:0/20:4)	0.77	0.51	0.66	0.140	0.041	0.101
PE(26:1/20:4)	0.67	0.66	0.97	0.053	0.067	0.455
PE(O-16:1/20:4)	1.11	1.26	1.14	0.182	0.114	0.250
PE(O-17:1/20:4)	1.01	0.90	0.89	0.459	0.274	0.246
PE(O-18:1/20:4)	0.95	0.91	0.95	0.335	0.253	0.356
PE(O-18:2/20:4)	0.99	1.09	1.10	0.438	0.328	0.304
PE(O-19:1/20:4)	0.62	0.42	0.68	0.074	0.099	0.220
PE(P-14:0/20:4)	1.10	0.84	0.76	0.307	0.151	0.124

PE(P-16:0/20:4)	0.90	1.11	1.23	0.396	0.397	0.272
PE(P-17:0/20:4)	0.94	0.80	0.85	0.344	0.222	0.290
PE(P-18:0/20:4)	0.83	0.66	0.80	0.088	0.047	0.160
PE(P-19:0/20:4)	0.62	0.42	0.68	0.084	0.088	0.209
PE(P-20:0/20:4)	0.84	0.81	0.96	0.116	0.119	0.398
PI(16:0/20:4)	**1.90**	**1.56**	**0.82**	**0.027**	**0.060**	**0.351**
PI(18:0/20:4)	**1.72**	**1.35**	**0.79**	**0.022**	**0.095**	**0.400**
PS(18:0/20:4)	1.14	0.98	0.86	0.203	0.465	0.284
TG(24:1_18:1_20:4)	0.44	0.32	0.73	0.015	0.021	0.166

Statistical evaluation was conducted using the Student's t-test. significant, P < 0.05, logFC<0.5 and logFC>2.0.

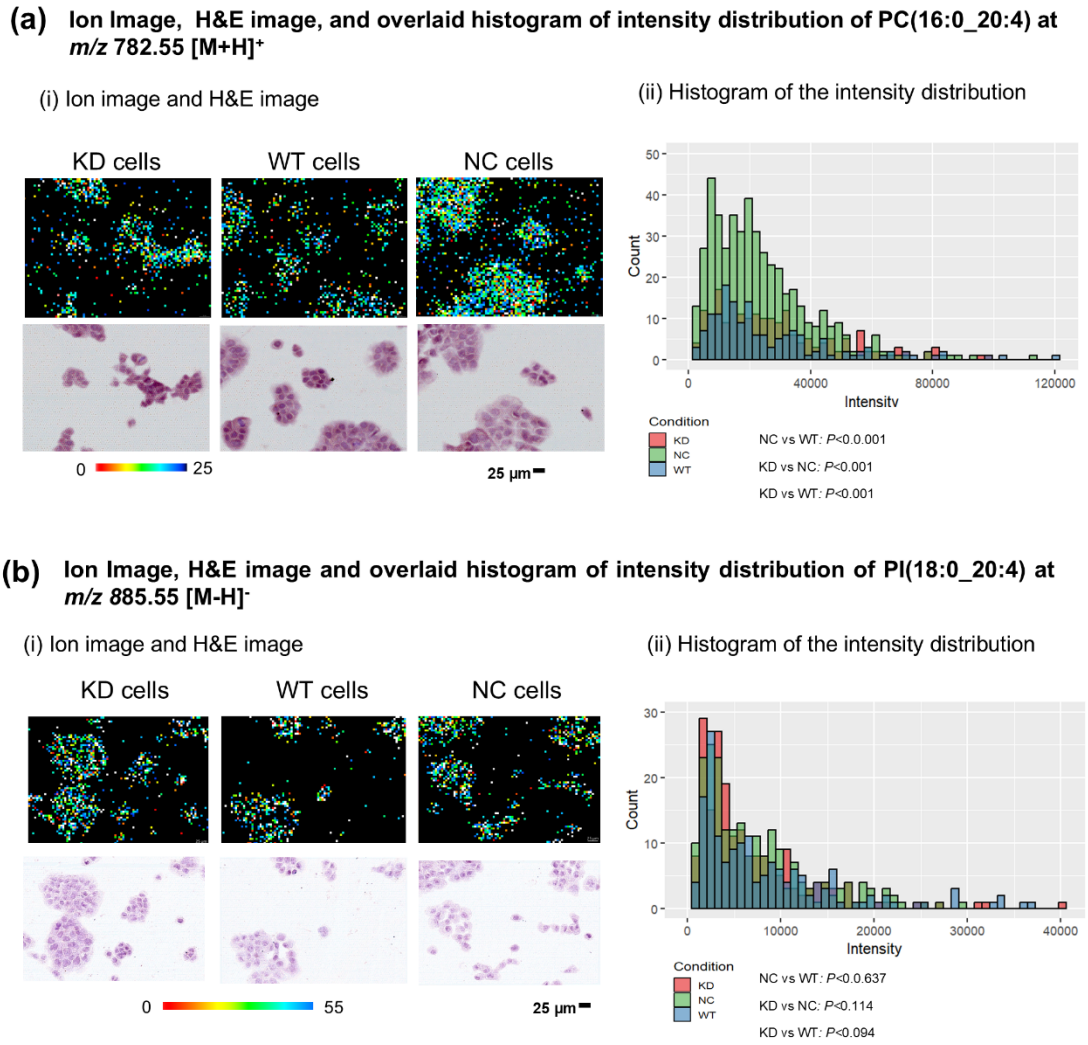

Fig. S7 Statistical analysis of the arachidonic acid-containing lipid molecules among KD, WT, and NC cells. **a** Ion image and histogram of the intensity distribution of PC (16:0/20:4) at the single-cell level analysis showed a significant difference in KD compared to WT and NC, but also showed a significant difference between WT vs NC. **b** Ion image and histogram of the intensity distribution of PC (18:0/20:4)

at the single-cell level analysis showed no significance among the groups. Kruskal-Wallis significance test. P. adj <=0.0001~****, P. adj <=0.001~***, P. adj <=0.01~**, P. adj <=0.05~*.

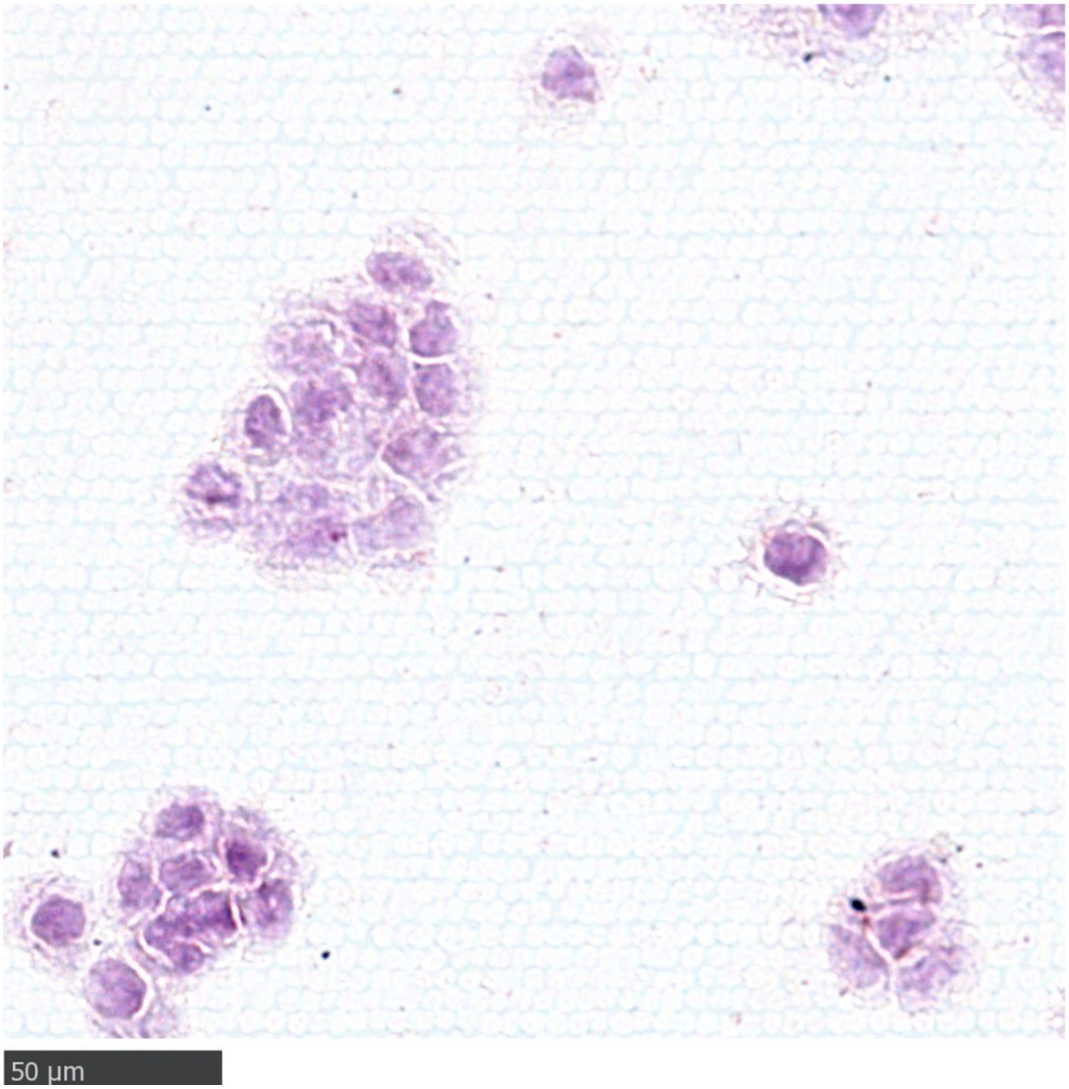

Fig. S8 H&E image showing the laser pixel within a cell

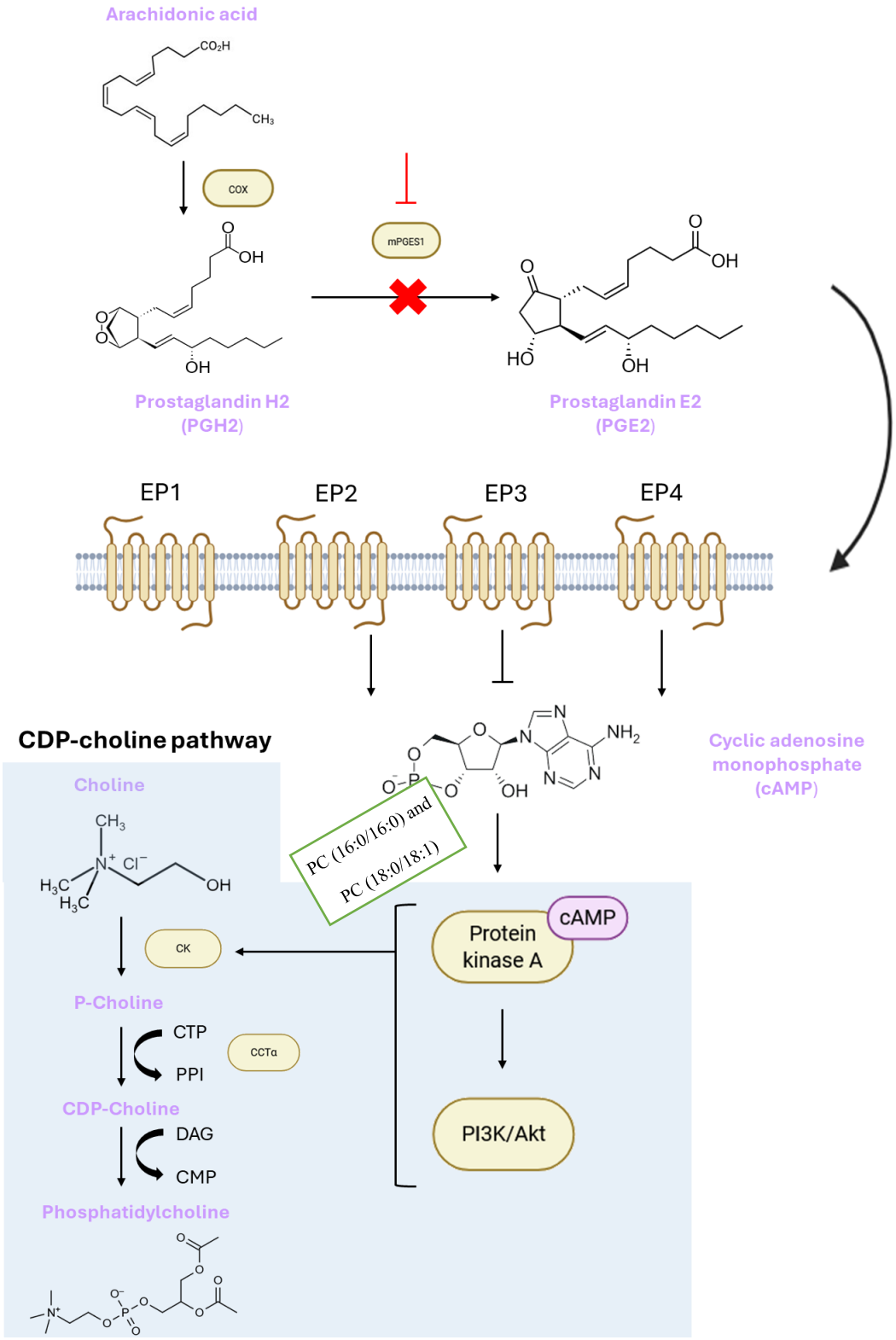

Fig. S9 Proposed mechanism of how mPGES-1 regulates PC metabolism. PGE2 exerts its role in phosphatidylcholine synthesis and its consequences in prostate cancer. PGE2 transmits its signal through G-protein-coupled cell surface receptors (EP1 to EP4). After PGE2 binding to the EP receptors, various

intracellular oncogenic pathways are stimulated. PGE2 binding with EP4 stimulated the PI3K/Akt pathway through cyclooxygenase pathways independently, which enhances the activity of choline kinase (CK) and Choline phosphate cytidylyltransferase-α (CCTα), resulting in the upregulation of PC biosynthesis. In hormone-resistant prostate cancer cell PC(16:0/16:1), PC(18:10/18:1) are markedly increased, but due to knockdown of the mPGES1 gene in hormone-resistant prostate cancer cells, these two lipids are significantly downregulated in the KD group compared to the WT and NC groups.